MDPI

Communication

Three-Dimensional Numerical Field Analysis in Transformers to Identify Losses in Tape Wound Cores

Dariusz Koteras * and Bronislaw Tomczuk

Department of Electrical Engineering and Mechatronics, Opole University of Technology, PL-45758 Opole, Poland; b.tomczuk@po.edu.pl
* Correspondence: d.koteras@po.edu.pl

Abstract: To find the total core losses in 1-phase medium-frequency transformers, a 3D numerical field analysis was carried out. The proposed numerical modeling was based on the extended iterative homogenization method (IHM) developed by the authors. The achieved calculation results were validated by the corresponding values obtained experimentally, and a reasonably close agreement was obtained.

1. Introduction

Many electrical devices were built using cores made of soft ferromagnetic materials. These cores were mainly manufactured either as laminated or as magnetically soft composites [1]. The soft magnetic materials are characterized by main parameters such as magnetic flux density B, magnetic field intensity H, and core losses P, as well as the magnetic permeability. Due to their application in many branches of industry, their properties can be significantly different [2–4]. In 2019, oriented steel was mainly used (at 60% share) in the global soft magnetic materials market; Figure 1 [5]. Lately, however, the sheets have been gradually replaced by amorphous ribbons, whereas ferrites, with a 13% share of the market, have taken second place.
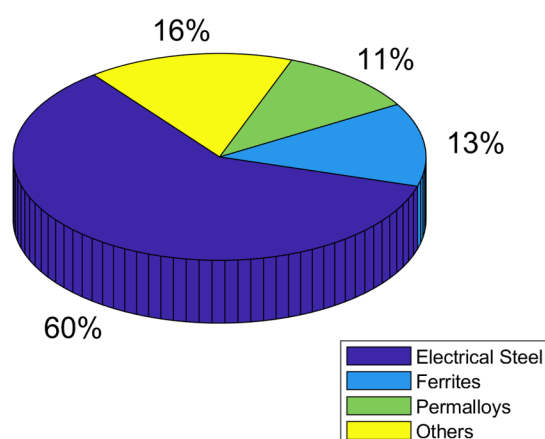

Figure 1. A pie graph for the global soft ferromagnetic materials market share in 2019.

The core losses inside magnetic materials are caused by two physical phenomena—eddy currents and hysteresis [6]. Inside the transformer's laminated core, the magnetic flux density vector is perpendicular to the smallest cross-section of the single sheet in the stack;

Figure 2. Under these operating conditions, the eddy current component of the losses can be found using the equation below:

$$P_{ec} = \int \frac{E^2}{R} dV \tag{1}$$

where E is the rms value of the electromotive force, R is the resistance of the single sheet, and V is the volume of the sheet.
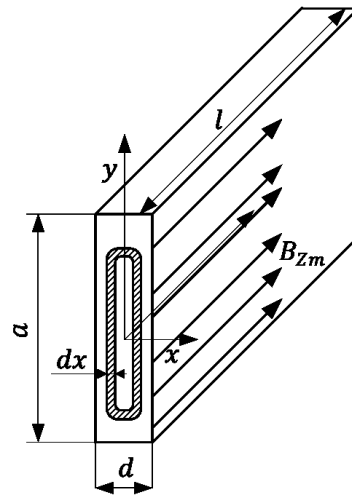

Figure 2. Assumed magnetic field conditions to calculate the eddy current losses component.

Calculation of the formula above leads to a well-known analytical expression for eddy current loss determination [7].

$$P_{ec} = \frac{1}{6}\sigma(\pi f B_{mav}d)^2 V \tag{2}$$

where σ is the electrical conductivity of the sheet, f is the frequency of the magnetic flux density, B_{mav} is the maximum value of the flux density in the cross-section of a sheet, and d is the thickness of the sheet.

Equation (2) concerns the linear model, which has been derived from the saturation-wave concept (SWM) by Wolman and Kaden [8]. In the literature [9,10], it has been proved that it is valid in the case where $B_p = B_m$. Thus, we have used it for the linear part of the magnetization curve.

The second phenomenon, i.e., hysteresis, has been investigated for many years. It can be described by two models: the Preisach and the Jiles–Atherton. The first model is described using an infinite set of simplest hysteresis operators $\hat{y}_{\alpha\beta}$, which represent the hysteresis nonlinearities. Each of these operators can be represented by the rectangular loop shown in Figure 3, [11]. Along with the set of operators $\hat{y}_{\alpha\beta}$, we use an arbitrary weight function $\mu(\alpha, \beta)$.

Using the presented above quantities, the so-called Preisach hysteresis operator $\hat{\Gamma}$ is defined as

$$\hat{\Gamma}u(t) = \int_{\alpha \geq \beta} \mu(\alpha, \beta)\hat{\mu}_{\alpha\beta}u(t)d\alpha d\beta \tag{3}$$

Applying this model in the numerical analysis of magnetic fields in ferromagnetic materials is widely described in the literature [12,13].

The second model of hysteresis described in the literature is the Jiles–Atherton model. It is based on the total differential susceptibility given in the below equation [14]:

$$\frac{dM}{dH} = 1 - c\frac{M_{an} - M_{irr}}{k\delta - \alpha(M_{an} - M_{irr})} + c\frac{dM_{an}}{dH} \tag{4}$$

where M_{an}—anhysteretic magnetization; M_{irr}—irreversible magnetization; δ—a directional parameter (+1, −1); k—coercivity; H_c—parameter; and α—coefficient of interdomain coupling in the magnetic material.
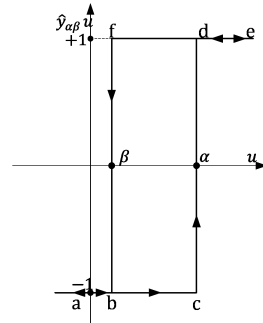

Figure 3. An elementary rectangular loop in the Preisach model.

Some parameters in this model, like α, k, and c, are obtained from the experimental data expressed through the form of a hysteresis loop [15]. This model is still used to calculate hysteresis in soft ferromagnetic materials [16]. Below are shown quite simple analytical formulas based on available measurement coefficients, i.e., Richter's and Steinmetz's approaches for hysteresis loss calculation [17]:

$$P_{hS} = \eta f B_{mav}^{1.6} m \tag{5}$$

$$P_{hR} = \varepsilon \frac{f}{100} B_{mav}^2 m \tag{6}$$

where η, ε—empirical coefficients; f—frequency of the flux change; B_{mav}—maximal average value of the flux density in the magnetic core; and m—the mass of the core.

There is a significant difference between the core loss values measured and those calculated with numerical field analysis and the analytical expressions. That difference is called the excess (auxiliary) losses component, P_{ex}. Thus, the total losses can be assumed to consist of three components: eddy current losses (P_{ec}), hysteresis ones (P_h), and those P_{ex}. The first interpretation of the excess losses was given by Pry and Bean who have taken into account the ratio $2L/d$ of the domain size (L) and the lamination thickness (d) [18]. However, their relationship includes too many simplifications and does not give reasonable accuracy. Below a more precise analytical expression is given in which the coefficients obtained from measurements can be applied. It is related to so-called active magnetic objects (MOs) of ferromagnetic materials [18,19].

$$P_{ax} = \frac{8 \cdot B_{mav} \cdot f \cdot m}{\rho} \left(\sqrt{\sigma \cdot G \cdot S \cdot B_{mav} \cdot f \cdot V_0} - \frac{\tilde{n}_0 \cdot V_0}{4} \right) \tag{7}$$

where B_{mav}—the maximal average value of the flux density in the core; S—the cross-sectional surface perpendicular to the flux direction in the core; G—the dimensionless coefficient (usually equal to 0.1356); $\tilde{n}_0$—the limiting number that characterizes the magnetic objects which are statistically independent when $f \to 0$; and V_0 is dependent on the $(H_{ax}, \tilde{n})$ function when $f \to 0$.

Nowadays, many electrical devices operate under medium frequencies, i.e., in the range of tens of kilohertz, which is much higher than the technical frequencies of 50 or 60 Hz. This results in smaller dimensions of the magnetic core geometry. However, for a medium-frequency core, the losses significantly increase. Thus, the proper values of appropriate loss must be predicted for these operating conditions when designing medium-frequency transformers.

For medium-frequency transformers, the analytical expressions concerning the core losses either do not exist or are given for selected frequency values only [2,3]. They are also inconvenient for direct use in numerical analysis, especially in 3D modeling, where instead of core lamination we should consider a solid structure of the magnetic circuit. Thus, in this paper we describe a 3D numerical analysis, based on our IHM [20,21], to calculate the total core losses inside the laminated core of the 1-phase transformer (Figure 4). In this method, the laminated core has been modeled as a solid structure with equivalent parameters such as conductivity σ_{eq} and relative magnetic permeability μ_{req}. In this method, the core is treated as a solid geometry with equivalent parameters (relative magnetic permeability and electrical conductivity). In the literature so far, the homogenization method mainly concerns simply laminated packages of grain-oriented silicon steels without measurement verification [22,23]. A significant part of this research concerns the numerical analysis of losses that occur in the transformer windings. For example, the paper in [24] numerically investigates the copper loss of a three-phase transformer dry-type 300 kVA under various geometry designs.
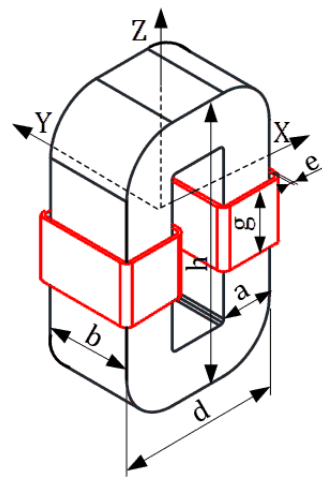

Figure 4. Outline of the analyzed objects.

2. Numerical Models

2.1. Analyzed Objects

This paper presents the results of our research concerning 1-phase transformers with a laminated "C"-type core made of two soft ferromagnetic materials; Figure 4.

The core of transformer T1 is made of the grain-oriented silicon steel OS-110 Cut "A" (GOSS), and the core of transformer T2 is made from amorphous ribbons of iron-based METGLAS® 2605SA1 [25,26]. For the 3D field analysis, a Cartesian coordinate system was assumed, as presented in Figure 4. According to it, the main dimensions of both transformers are given in Table 1.

Table 1. Main dimensions of the transformers (in [mm]).

Symbol	Transformer 1	Transformer 2
a	24	16
b	40	40
d	75	52
h	128.6	102
e	1.35	1.35
g	29	29

To facilitate the calculations, instead of the layered core, we considered its modular structure, in the "C" letter form, of two solid parts. Additionally, to avoid losses in the

transformer windings (coils), we used Litz wire. Both windings, with the same number of turns ($N = 21$), were connected in series.

2.2. Numerical Model

Our numerical analysis used the Maxwell 3D module from the commercial Ansys simulation package. In this package, the Finite Element Method is implemented using automatic mesh generators. Therefore, interference in the density of the discretization mesh is limited. However, within the Maxwell 3D package, it is possible to refine the mesh on the boundaries of the object and subareas by specifying the length of the elements. In Figure 5a,b, the finite element grids generated for the two transformers are shown. The total number of elements in the grid is equal to 39,158 for the transformer T_1 (with GOSS) and 16,497 for the T_2 amorphous one. The correctness of the simulations is achieved after obtaining the previously assumed energy error. They were executed in four passes for the first transformer and three passes for the second one.
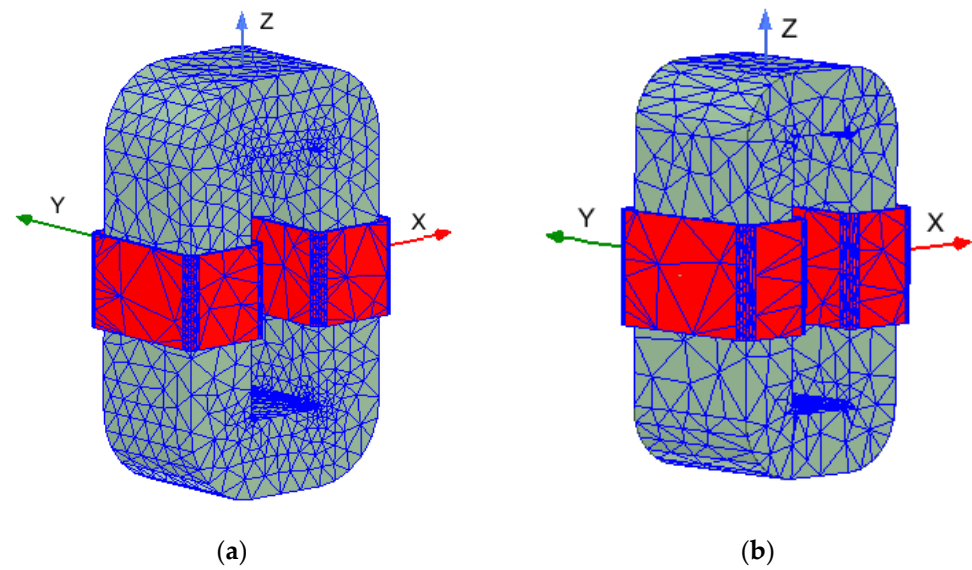

(**a**) (**b**)

Figure 5. Finite element grids: (**a**) for transformer T_1; (**b**) for transformer T_2.

For the 3D calculation, we investigated the eddy current models with the frequency domain. The algorithm of the solver is based on the T–Ω formula, where T is an electric vector potential and Ω is a magnetic scalar potential [27,28]. Obviously, the non-conducting regions hold the below equation:

$$div(grad\Omega) = 0 \tag{8}$$

In the regions with non-zero conductivity, where eddy currents flow, the below equation must be solved:

$$\Delta T = j\omega\mu\sigma_{eq}(H_S + T - grad\Omega) \tag{9}$$

where σ_{eq} is the equivalent conductivity of the solid core and μ is the magnetic permeability of it; H_S is magnetic field strength excited by the coils.

Below are given, implemented in Ansys software, version R1 from 2020 the relationships for each component of the losses:

$$P_{ec} = K_{ec}f^2B_{mav}^2 \tag{10}$$

$$P_h = K_hfB_{mav}^2 \tag{11}$$

$$P_{ax} = K_{ax}f^{1.5}B_{mav}^{1.5} \tag{12}$$

To calculate the total core losses based on the proper value of each coefficient, K_{ec} for eddy currents, K_h for hysteresis and K_{ex} for excess losses, our modified IHM was applied. A simplified flow chart of that algorithm is given in Figure 6.
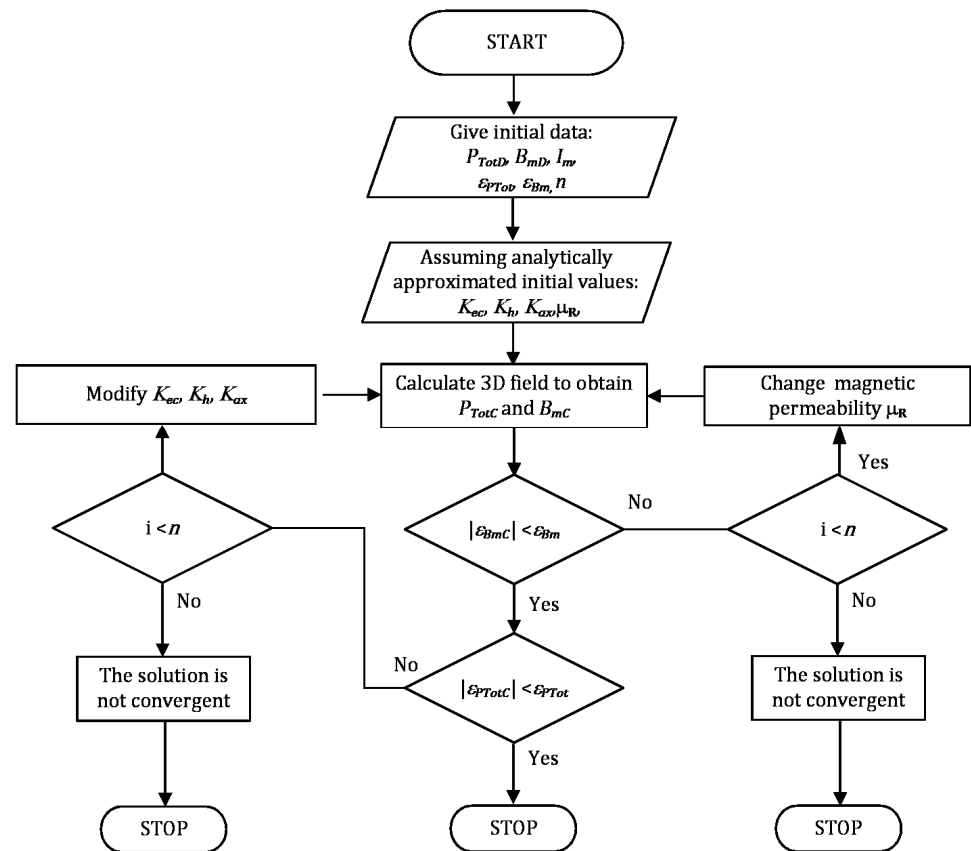

Figure 6. Flow chart of the algorithm for modified IHM.

Firstly, the P_{TotD}, i.e., total losses of the transformer, and B_{mD}, i.e., the magnetic flux density maximal average value, are assumed. These values, inside the core, are related to the operating conditions of the transformer. At the start of the solver execution, the transformer's operating conditions and maximal number n of iterations are assumed. The algorithm starts with assumed initial values for each coefficient K_{ec}, K_h, and K_{ax}. After the magnetic field analysis, we verified the value of magnetic flux density inside the core. When its estimation is correct, i.e., the relative error of the magnetic flux density ε_{Bm} is lower than the assumed one, the value of the total loss is checked. When this value is appropriate, i.e., the relative error of the total core losses ε_{Bm} is lower than that assumed, the algorithm stops the iterative process. Finally, when the calculations reach the n number of iterations, it will be also stopped to prevent continuous looping.

Our numerical model extends the application of the IHM method described in [16]. In this model, we have assumed the equivalent conductivity of the core (at $\sigma_{eq} = 700$ S/m). This value was valid for the entire core, in which an almost constant value of the magnetic flux density was maintained (Figure 7a,b). It gives a good approximation to the real laminated cores, where each single sheet has a similar B_{mav} value inside the core. On the other hand, the equivalent relative permeability μ_{req} was selected in an iterative process to make it possible to obtain the same average value of the magnetic flux density B_{mav} in the cross-sectional plane halfway up the transformer column.
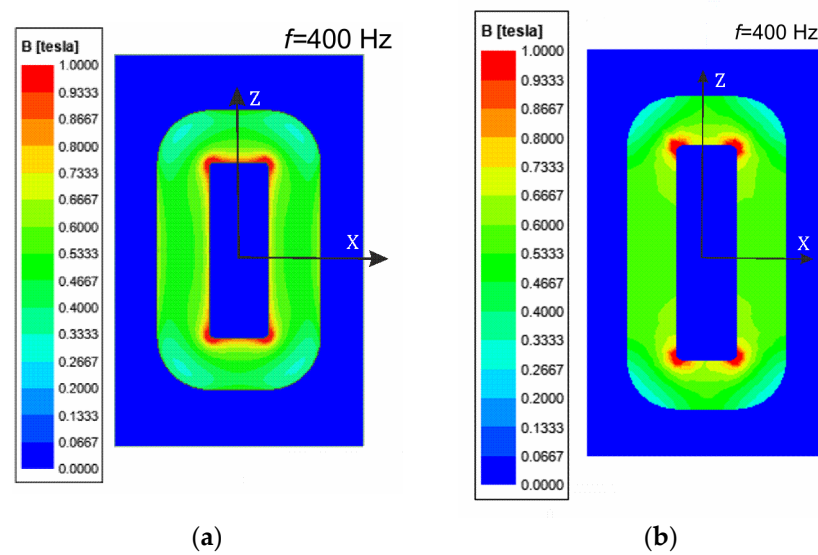
Figure 7. The *B* distribution inside the core on the XZ plane: (**a**) for transformer T_1; (**b**) for transformer T_2.

3. Calculation Results and Measured Verification

In our numerical analysis, the investigated transformer was powered by sinusoidal current waves of frequencies ranging from 50 Hz to 400 Hz.

Due to the overheating of the core during measurements at the increased frequency, the tests were carried out for relatively low values of flux density. The presented calculation results of the core losses were given at the value of B_{mav} = 0.6 T and the excitation current wave frequency of f = 400 Hz. The magnetic flux density *B* module is presented in Figure 7a,b by the color bitmaps used for the *B* module distribution inside the core's *XZ* plane (Figure 4). Note that the maximum values of *B* are in the subregions near the corners of the transformer window. In contrast, the minimum ones are in the outer part of the core corners. In the columns and yokes, the *B* values are almost equal. For the transformer T_1, the P_{ec} component has been included in the total losses. Thus, in Figure 8, the eddy current *J* distribution is presented inside the *XZ* plane.
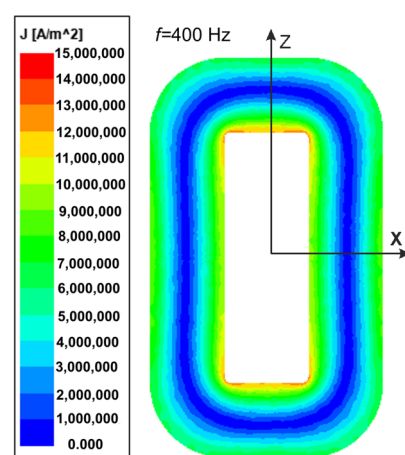

Figure 8. The eddy current density *J* distribution inside the *XZ* plane of the transformer T_1 core.

Figure 9a,b show components of the total losses for transformer (GOSS) T_1 vs. frequency. In Figure 9a the percentage share for each component of the total losses is presented, whereas Figure 9b gives the values of each component. As can be seen, for the frequency equal to f = 50 Hz, the components caused by the eddy currents dP_{ec} and hysteresis dP_h phenomena have the same percentage share, which equals approximately 30% of the total

losses. For the gradually increased value of the frequency, the component dP_{ec} significantly increases until its percentage share achieves about 80%.
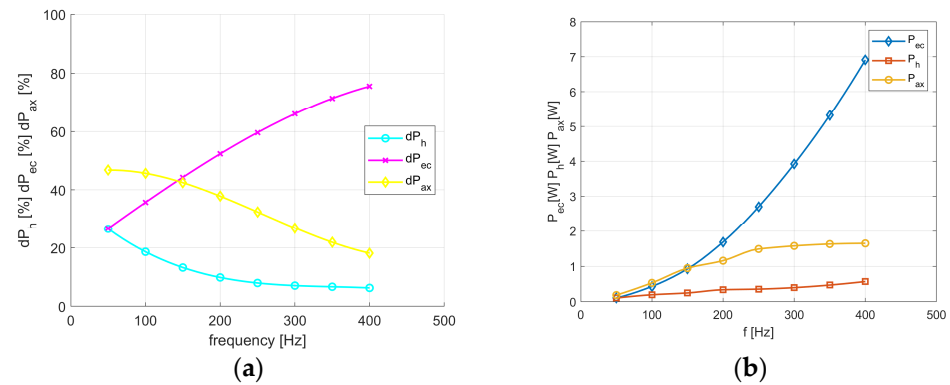

Figure 9. Components of the total losses for transformer T_1 vs. frequency: (**a**) percentage share of the total losses components; (**b**) values of each component.

Although the total losses in transformer T_2 are determined correctly, their division for the amorphous package seems to be slightly erroneous. Due to the narrow hysteresis loop of amorphous materials in the considered frequency range, the hysteresis losses in the T_2 transformer are much lower than those in transformer T_1 (from GOSS). Moreover, the losses from eddy currents, calculated by Equation (2), constitute approximately 1% of the total losses [29]. However, the measurement results give higher values. Additionally, the loss components defined by Formulas (10)–(12) also contribute to the power share components imprecisely. These calculations show that auxiliary losses account for almost all of the total ones, which seems slightly strange and will be the subject of our further research.

Figure 10a,b present the measured core losses for the entire scope of our tests. For the frequencies from 50 up to 400 Hz and the magnetic flux density from 0.1 up to 1.2 T, calculations are included for the transformer T_1 (with GOSS core), and the flux density from 0.1 up to 1.0 T for the amorphous object for the transformer T_2 was obtained. It can be noticed that the maximum value of the losses for the amorphous core is about three times lower.
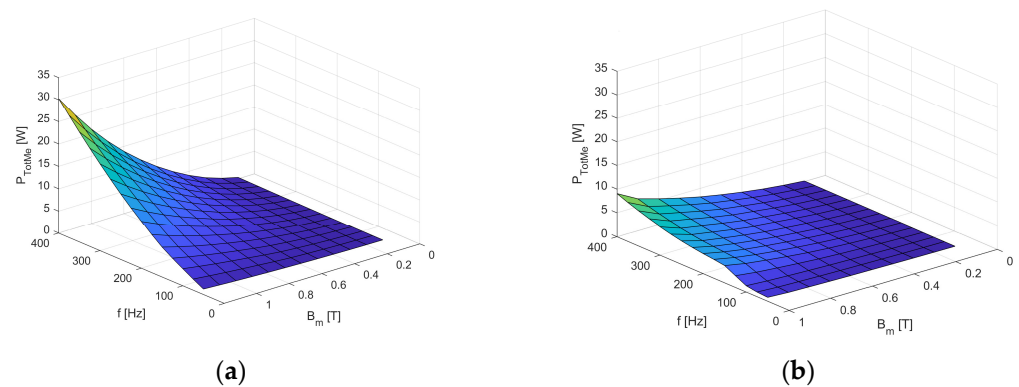

Figure 10. Relationship $P_{TotMe} = f(f, B_m)$: (**a**) for transformer T_1; (**b**) for transformer T_2.

As mentioned above, the total core losses in transformer T_1 (with GOSS) consist of all three components, whereas in amorphous transformer T_2, the P_{ax} component seems to be a decisive part of the total losses. Thus, Figure 11a,b give the coefficients, calculated with the IHM algorithm, occurring in Equations (10)–(12). However, the measurement results for transformer T_2 give higher values of the hysteresis and eddy current losses than the calculated ones. Moreover, the loss components defined by Formulas (10)–(12) also contribute to the power share components imprecisely. These calculations show that

auxiliary losses account for almost all of the total ones, which seems slightly strange and will be the subject of our further research.
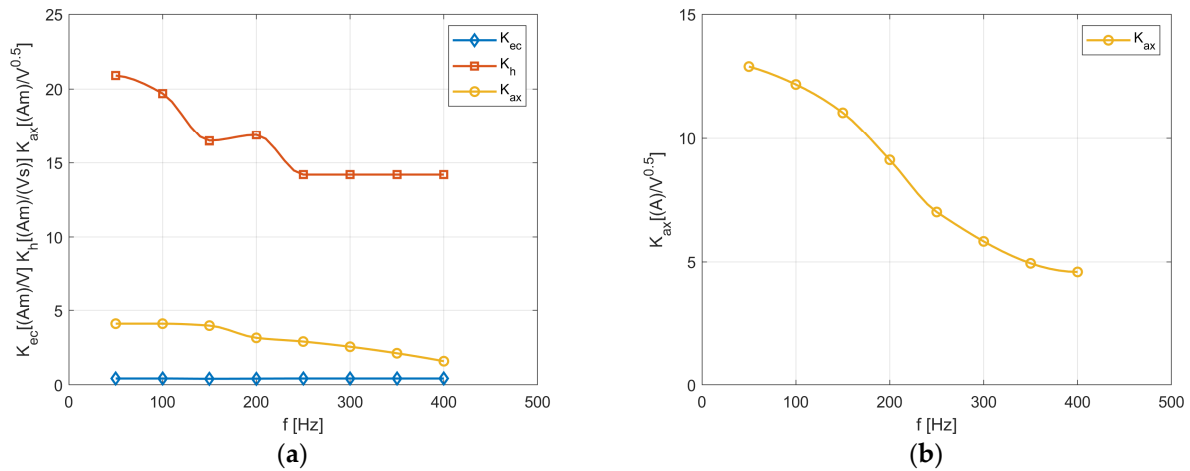

Figure 11. Comparison of the calculated and measured total losses: (**a**) for transformer T_1; (**b**) for amorphous transformer T_2.

The linearity of the K_{ec} characteristic results from analytical Equation (2) and from that implemented in (10). From the relationships, it is visible that the frequency f exponent and the magnetic flux density B_{mav} are the same value and equal to 2. The decreasing values of the other coefficients result from the fact that the component losses have a lower share in the total losses (Figure 9). Moreover, the values of the frequency f exponent and the flux density B_{mav} differ in the analytical and the numerically implemented equations. Similarly, in the amorphous transformer (T_2), the graph of the K_{ax} values results from the fact that the total losses versus the frequency values increase due to the linear approach (Figure 10b), whereas using Equation (12), the losses change non-linearly due to the exponent number, which is equal, i.e., 1.5, vs. the frequency function.

Our numerical analysis was verified by the measurement tests with the 8-bit digital oscilloscope Tektronix MSO 2024B. The simplified diagram of the measurement system is given in Figure 12. Figure 13a,b show the calculated and measured values of the iron losses versus frequency values *f*. Our calculations give the possibility to determine the losses for other frequencies, where the material parameters of solid cores were determined based on the approximation between the nodes of the interactive process, where the total discrepancy between measurements and loss calculations is visible. Figure 13a,b show a comparison of the calculated and measured values of the total losses for both analyzed transformers. The small differences of about 10% between the values given in these figures validate our modeling of the losses in the laminated core.
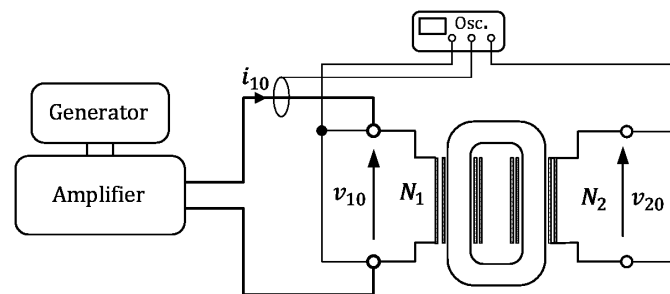

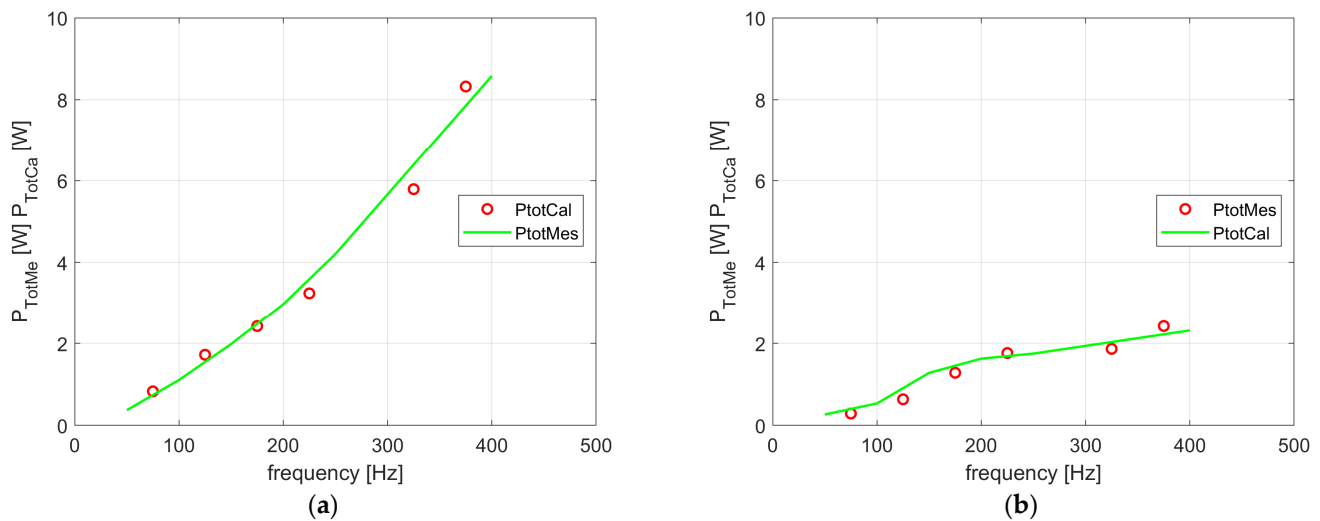**Figure 12.** The simplified diagram for measurement of the total core losses.

Figure 13. Comparison of the calculated and measured total losses: (**a**) for transformer T_1; (**b**) for transformer T_2.

4. Conclusions

In the currently published approaches, the design of electromagnetic devices is supported by 3D numerical field analysis. Proper modeling for each separate sheet, or a strip of it, in the laminated core is almost impossible. Therefore, in this paper, we describe calculation models with solid core geometry. Our iterative numerical approach is based on mathematical modeling with the equivalent parameters, such as the conductivity σ_{eq} and the relative magnetic permeability μ_{req}, of the core. In our analysis, described herein, the proper values of the coefficients (K_{ec}, K_h, and K_{ax}) for each component of the core losses have been calculated. The correctness of the presented models has been validated by the measurements, and a satisfying convergence of results for both models was reached (Figure 13a,b). Consequently, we recommend the proposed IHM method as applicable in calculations of both GOSS sheets, with their domain structure, and amorphous ribbons.

References

1. Mazaleyrat, F. Soft Magnetic Materials. In *Handbook of Magnetism and Magnetic Materials*; Coey, M., Parkin, S., Eds.; Springer: Cham, Switzerland, 2021. [CrossRef]
2. Available online: https://www.femag.it/wp-content/uploads/2022/12/femag_lamiere_silicio.pdf (accessed on 4 May 2023).
3. Available online: https://metglas.com/magnetic-materials/ (accessed on 4 May 2023).
4. Available online: https://ferroxcube.home.pl/prod/assets/sfmatgra_frnt.pdf (accessed on 4 May 2023).
5. Available online: https://www.grandviewresearch.com/industry-analysis/soft-magnetic-materials-market (accessed on 25 January 2023).
6. Bozorth, R.M. *Ferromagnetism*; Wiley & Sons Inc.: Hoboken, NJ, USA, 2003.
7. Bertotti, G. *Hysteresis in Magnetism*; Academic Press: San Diego, CA, USA, 1998.

8.   Wolman, W.; Kaden, H. Über die Wirbelstromverzögerung Magnetisehe Schaltvorgänge. *Z. Tech. Phys.* **1932**, *13*, 330–345.

9.   Bertotti, G. *Hysteresis in Magnetism for Physicists, Materials Scientists, and Engineers*; Academic Press: San Diego, CA, USA, 1998.

10.   Mayergoyz, I.D.; Serpico, C. Eddy-current losses in magnetic conductors with abrupt magnetic transitions. *IEEE Trans. Magn.* **2000**, *36*, 1962–1969. [CrossRef]

11.   Mayergoyz, I. *Mathematical Models of Hysteresis and Their Applications*; Elsevier: Amsterdam, The Netherlands, 2003.

12.   Hussain, S.; Lowther, D.A. An Efficient Implementation of the Classical Preisach Model. *IEEE Trans. Magn.* **2018**, *54*, 7300204. [CrossRef]

13.   Mörée, G.; Leijon, M. Review of Play and Preisach Models for Hysteresis in Magnetic Materials. *Materials* **2023**, *16*, 2422. [CrossRef] [PubMed]

14.   Jiles, D.C.; Ramesh, A.; Shi, Y.; Fang, X. Application of the Anisotropic Extension of the Theory of Hysteresis to the Magnetization Curves of Crystalline and Textured Magnetic Materials. *IEEE Trans. Magn.* **1997**, *33*, 3961–3963. [CrossRef]

15.   Jiles, D.C.; Thoelke, J.B.; Devine, M.K. Numerical Determination of Hysteresis Parameters the Modeling of Magnetic Properties Using the Theory of Ferromagnetic Hysteresis. *IEEE Trans. Magn.* **1992**, *28*, 27–35. [CrossRef]

16.   Malczyk, R.; Izydorczyk, J. The frequency–dependent Jiles–Atherton hysteresis model. *Physica B* **2015**, *463*, 68–75. [CrossRef]

17.   Kollár, P.; Vojtek, V.; Birčáková, Z.; Füzer, J.; Fáberová, M.; Bureš, R. Steinmetz law in iron–phenolformaldehyde resin soft magnetic composites. *J. Magn. Magn. Mater.* **2014**, *353*, 65–70. [CrossRef]

18.   Bertotti, G. General properties of power losses in soft ferromagnetic materials. *IEEE Trans. Magn.* **1988**, *24*, 621–630. [CrossRef]

19.   Bertotti, G. Direct relation between hysteresis and dynamic losses in soft magnetic materials. *J. Phys.* **1985**, *46*, 389–392. [CrossRef]

20.   Koteras, D.; Tomczuk, B.; Waindok, A. Implicit iteration calculations using 3D field analyses, to predict the power loss in powder ferromagnets, with their measurement tests. *Measurements* **2023**, *207*, 112311. [CrossRef]

21.   Koteras, D.; Tomczuk, B. Comparison of the field methods in homogenization of the laminated magnetic cores. *Int. J. Appl. Electromagn. Mech.* **2020**, *63*, 705–714. [CrossRef]

22.   Krähenbühl, L.; Dular, P.; Zeidan, T.; Buret, F. Homogenization of lamination stacks in linear magnetodynamics. *IEEE Trans. Magn.* **2004**, *40*, 912–915. [CrossRef]

23.   Gyselinck, J.; Sabariego, R.V.; Dular, P. A nonlinear time-domain homogenization technique for laminated iron cores in three-dimensional finite-element models. *IEEE Trans. Magn.* **2006**, *42*, 763–766. [CrossRef]

24.   Chiu, H.-C.; Pao, H.-K.; Hsieh, R.-H.; Chiu, Y.-J.; Jang, J.-H. Numerical Analysis on the Eddy Current Losses in a Dry-type 3000 kVA Transformer. *Energy Procedia* **2019**, *156*, 332–336. [CrossRef]

25.   Available online: https://www.femag.it/en/products/cores-c-series/ (accessed on 13 April 2024).

26.   Available online: https://metglas.com/distribution-transformer-electrical-steel/ (accessed on 13 April 2024).

27.   Maxwell Help, Ansys 2020 R1. 2020. Available online: https://www.ansys.com/it-solutions/contacting-technical-support/ (accessed on 15 May 2024).

28.   Wajnert, D. A field-circuit model of the hybrid magnetic bearing. *Arch. Mech. Eng.* **2019**, *66*, 191–208. [CrossRef]

29.   Masood, A.; Baghbaderani, H.A.; Alvarez, K.L.; Blanco, J.M.; Pavlovic, Z.; Ström, V.; Stamenov, P.; Mathuna, C.O.; McCloskey, P. High-frequency power loss mechanisms in ultra-thin amorphous ribbons. *J. Magn. Magn. Mater.* **2021**, *519*, 167469. [CrossRef]